

See discussions, stats, and author profiles for this publication at: <https://www.researchgate.net/publication/221720260>

Modification of Gold Catalysis with Aluminum Phosphate for Oxygen–Reduction Reaction

ARTICLE *in* THE JOURNAL OF PHYSICAL CHEMISTRY C · MARCH 2010

Impact Factor: 4.77 · DOI: 10.1021/jp9103323

CITATIONS

28

READS

45

7 AUTHORS, INCLUDING:



Chunjoong Kim

University of Illinois at Chicago

59 PUBLICATIONS 1,372 CITATIONS

[SEE PROFILE](#)



Jongmin Kim

Seoul National University

33 PUBLICATIONS 727 CITATIONS

[SEE PROFILE](#)



Yuhong Oh

Seoul National University

12 PUBLICATIONS 182 CITATIONS

[SEE PROFILE](#)

Modification of Gold Catalysis with Aluminum Phosphate for Oxygen-Reduction Reaction

Yejun Park, Byungjoo Lee, Chunjoong Kim, Jongmin Kim, Seunghoon Nam, Yuhong Oh, and Byungwoo Park*

Department of Materials Science and Engineering, Research Center for Energy Conversion and Storage, and Research Institute of Advanced Materials, Seoul National University, Seoul 151-744, Korea

Received: October 29, 2009; Revised Manuscript Received: January 25, 2010

The activities of Au/AlPO₄ nanocomposites with the variation of metal phosphates were examined for oxygen-reduction reactions, both in an alkaline and acidic environment. In an alkaline media, the activities of the Au/AlPO₄ nanocomposites on the oxygen-reduction were enhanced. The steeper reduction slope as well as larger reduction current density were observed in the potential range of approximately 0.8–1.0 V (vs reversible hydrogen electrode) with the newly appeared peak at ~0.85 V. In an acidic media, the oxygen reduction on the Au/AlPO₄ nanocomposites presented both higher onset potential and steeper reduction slope than that on the Au catalyst. Such enhancements were attributed to the electronic interactions between Au and AlPO₄, as confirmed by X-ray photoelectron spectroscopy.

Introduction

Low temperature fuel cells have been extensively researched including the existing proton-exchange-membrane fuel cells (PEMFCs) which are operated in an acidic environment.^{1–3} Recently, research of catalysts on alkaline environment has increased for applications, such as direct borohydride fuel cells and alkaline direct methanol fuel cells.^{4,5} The progress of the oxygen-reduction ($O_2 + 4H^+ + 4e^- \leftrightarrow 2H_2O$, $E = 1.23$ V vs RHE) catalyst is important because oxygen (or air) is a unique chemical source for the reduction reaction as opposed to several anode fuels, such as hydrogen, borohydride, small organic molecules, etc.^{3,4,6} There are a number of concerns associated with oxygen-reduction reaction (ORR) under various conditions, including different activity in several environments like acid or alkaline solutions, and the catalytic selectivity to certain chemical reactions.^{7,8} Non-platinum catalyst is one of the most tempting issues from the basic research of catalysis to the price competitiveness of fuel cells. Non-platinum catalysts and low platinum-loaded catalysts have been extensively explored with various nanostructures.^{9,10}

Gold is an unusual catalyst in terms of its inertness in the bulk state and its catalytic activity with specific nanostructures. The catalytic nature of gold has been found to be tunable through the control of the nanoparticle size, the selection of the matrix materials, and the nanostructures of the metal–matrix composites.¹¹ Exceptional catalytic activities of oxide-supported gold nanoparticles have been reported in conjunction with the oxygen reduction, CO oxidation, etc.^{12,13} Interactions with the matrix materials can modify the electronic structure of Au, as well as the chemisorption characteristics of the reactants.^{14,15} In this article, we report that the catalytic activities of Au for ORR can be enhanced with Au/AlPO₄ nanocomposites both in an alkaline and acidic environment.

Metal phosphate was selected as a matrix material as it offers resistance to dissolution under the corrosive conditions of the fuel cell cathode, while providing oxygen permeability owing to its porous nature.¹⁶ Nanoporous structures of amorphous (or

poor-crystalline) metal phosphates allow suitable transfer of protons, water, methanol, and oxygen.^{17–19} The composite nanostructures offer the advantage of forming a large interfacial area, and also facilitate charge transfers between gold and phosphate.

To modify the metal phosphate as a matrix material, the deposition pressure was varied. At high operating pressure, thermalization of sputtered species occurs from their kinetic energy loss due to an increase in collision frequency. The energy of arriving atoms is lowered with approximately 1 order of magnitude within the pressure range (5–45 mTorr) used in this article, according to the Monte Carlo simulation of Yamamura et al.²⁰ The sputtered species interact with the ionized/excited gas molecules and electrons in the plasma, and their chemical or electronic states can be changed depending on the density of plasma. The various sputtered species at different operating pressures can influence the chemical configurations, defect densities like oxygen vacancies, and electronic structures of the deposited metal phosphates.

Experimental Procedure

The Au/AlPO₄ nanocomposite was deposited on indium–tin oxide (ITO) coated glass (Samsung Corning) by rf magnetron sputtering with Au and AlPO₄ targets. The deposition was performed at room temperature (RT) under an Ar atmosphere with varying operating pressures of 5, 25, and 45 mTorr for Au/AlPO₄ nanocomposites and 25 mTorr for Au electrodes. The varied Au/AlPO₄ nanocomposites were annealed at 200 °C for 30 min under vacuum for the desired adhesion onto the ITO electrodes. The Au electrodes were annealed under the same conditions for direct comparison. To compare the ORR activities, Pt electrodes were also prepared.¹⁷

Electrochemical measurements were made with an electrochemical analyzer (CHI 604A, CH Instrumental Inc.) using a conventional three-electrode configuration at RT. The Au or Au/AlPO₄ nanocomposite electrodes, Pt wire, and saturated calomel electrode (SCE) were served as the working, counter, and reference electrodes, respectively. All the potentials have been converted and are presented vs reversible hydrogen electrode (RHE) in this article. The electrochemical properties

* To whom correspondence should be addressed. E-mail: byungwoo@snu.ac.kr. Phone: +82-2-880-8319. Fax: +82-2-885-9671.

without oxygen were determined with cyclic voltammetry at a scan rate of 50 mV/s in a nitrogen-purged 0.5 M H₂SO₄ solution. The electrochemical surface area can be estimated from the electric charge for the reduction peak of the chemisorbed oxygen on a gold surface (Au—O).²¹ The ORR activities were examined with cyclic voltammetry at a scan rate of 50 mV/s in an oxygen-saturated 0.5 M H₂SO₄ or 1 M NaOH solution. Electrochemical impedance spectroscopy was performed in an oxygen-saturated 0.5 M H₂SO₄ solution at 0.38 V with the amplitude of 0.05 V in the frequency range from 0.05 Hz to 100 MHz. The oxygen flow was fixed at 50 sccm during the ORR measurement.

The nanostructures were analyzed by transmission electron microscope (TEM, Tecnai F20, Philips/FEI), and samples were prepared by peeling off the catalyst layer after repeated potential cycling (0.2–1.6 V vs RHE in a 0.5 M H₂SO₄) and placing it on a 200 mesh copper grid (TED PELLA, INC. Prod No. 01800). The grain size and phase were determined by X-ray diffraction (XRD, M18XHF-SRA, MAC Science) with Cu K α radiation ($\lambda = 0.15418$ nm). The grain sizes were estimated using the Scherrer formula.²² The peak widths (full width at half-maximum) were fitted using a double peak Lorentzian function, considering the effect of K α_1 and K α_2 . To correct the instrumental broadening effect, a resolution function estimated from a silicon powder (Aldrich) was subtracted after fitting for each peak. The surface plasmons of gold nanocrystallites within the Au/AlPO₄ nanocomposites were examined using an UV spectrometer (Cary 5000; Varian) with a tungsten-halogen lamp source. The surface morphology was observed with atomic force microscopy (AFM, SPA-400, Seiko). X-ray photoelectron spectroscopy (XPS, Sigma Probe: Thermo VG Scientific) was used to analyze the electronic structure both in the core and valence band states with monochromatic Al K α radiation. The binding energy scale was calibrated by setting the C 1s peak at 285.0 eV.²³ An inductively coupled plasma-atomic emission spectrometer (ICP-AES, Optima-4300 DV, Perkin-Elmer) was used to determine the ratio of Au/Al in the Au/AlPO₄ nanocomposites. Fourier-transform infrared spectroscopy (FT-IR, Nicolet 5700, Thermal Electron) was used for observing the nanostructures from the various AlPO₄ samples.

Results and Discussion

The TEM image (Figure 1a) represents the facets and cusps of several nanometer-sized gold grains in the Au/AlPO₄ nanocomposite. The size of gold grains is consistent with the XRD analysis (shown in Figure 2a). The gold grains have sizes of 8.2 ± 0.4 , 6.7 ± 0.4 , and 10.9 ± 0.7 nm, respectively, in the Au/AlPO₄ nanocomposites deposited at the pressures of 5, 25, and 45 mTorr. The grain sizes of gold in the Au/AlPO₄ composites are smaller than those of the deposited gold alone (19.8 ± 0.2 nm). The changed grain size in the nanocomposites is thought to be induced by the interposed AlPO₄ between the gold grains. No distinct crystalline peaks other than Au were observed, demonstrating the amorphous (or poor-crystalline) nature of aluminum phosphate (JCPDS 46-0695).

The high angle annular dark field (HAADF) image (Figure 1b) indicates that gold nanocrystallites form a somewhat aggregated and connected geometry, demonstrating both feasible electronic conduction of gold and suitable transport of the reactants. These nanostructures are also identified by the surface plasmon in the absorption spectra of Figure 2b. The Au/AlPO₄ nanocomposites show a surface plasmon peak at ~ 650 nm, while the gold thin film does not show any localized surface plasmon peak.²⁴ A single peak is observed at 600–700 nm for gold nanoparticles with a diameter ranging from a few nano-

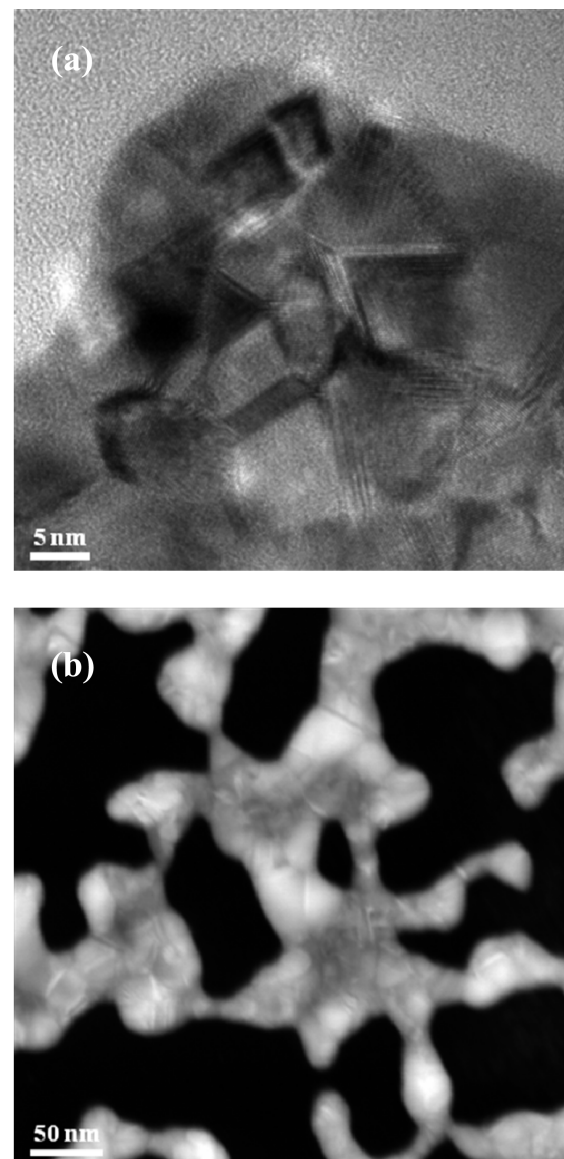


Figure 1. (a) High resolution TEM image and (b) HAADF (Z-contrast STEM) image of the Au/AlPO₄ nanocomposite deposited at the working pressure of 25 mTorr.

meters to ~ 50 nm.^{25–27} From ICP-AES, the Au/Al atomic ratio was ~ 10.5 , ~ 11.5 , and ~ 10.6 , respectively, for the deposition pressures of 5, 25, and 45 mTorr. The volume fraction of Au in the Au/AlPO₄ nanocomposites is at most $\sim 70\%$, depending on the porosity of the deposited AlPO₄ matrix.

The Au and Au/AlPO₄ nanocomposites display different surface morphologies, as shown in AFM images (Figure S1). The cross-sectional line profile of each sample indicates that the Au/AlPO₄ nanocomposites have a more laterally wrinkled surface than the gold sample. The wrinkled surface leads to higher active surface areas for the catalyst. The active surface area of gold can be electrochemically estimated from the reduction peak at ~ 1.2 V of the chemisorbed oxygen on a gold surface (Au—O) in the cyclic voltammogram, even with some inaccurate coverage of the chemisorbed oxygen on the gold surface.²⁰ As shown in Figure S2, the reduction peak areas of the chemisorbed oxygen on nanocomposites are larger than Au thin film by a factor of ~ 2.6 , ~ 2.9 , and ~ 2.5 , respectively, depending on the deposition pressures of 5, 25, and 45 mTorr.

To examine the catalytic activities of Au and the Au/AlPO₄ nanocomposites, their ORR currents were recorded with cyclic

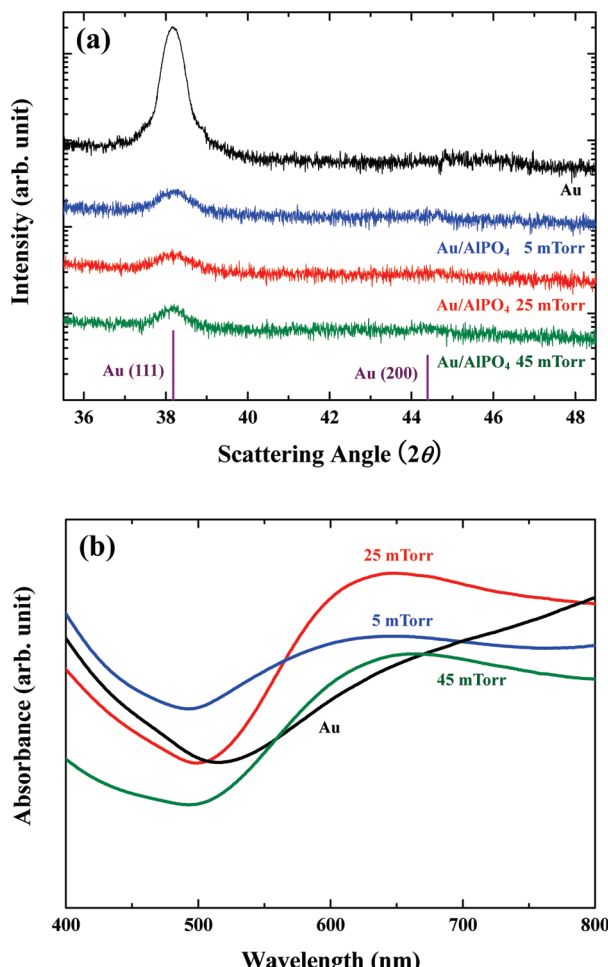


Figure 2. (a) XRD patterns and (b) absorption spectra of the Au thin film and Au/AlPO₄ nanocomposites, deposited at the working pressures of 5, 25, and 45 mTorr, respectively. The XRD gold peaks are identified as crystalline Au (JCPDS 04-0784). The absorption peaks at ~650 nm indicate a surface plasmon of gold nanoparticles.²⁵

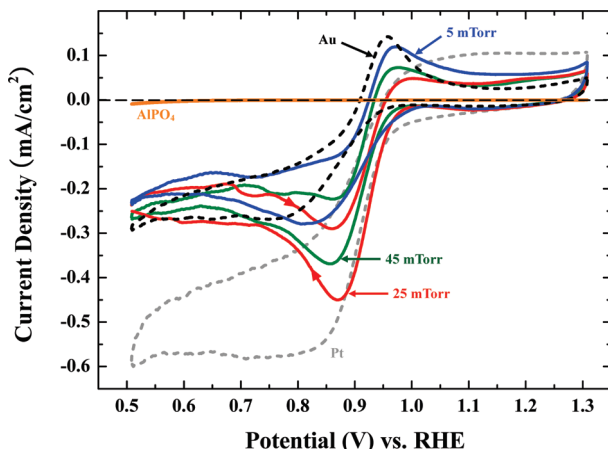


Figure 3. Oxygen-reduction activities of the Au/AlPO₄ nanocomposite, Au, and AlPO₄ electrodes in the oxygen-saturated 1 M NaOH solution at a scan rate of 50 mV/s.

voltammetry in an oxygen-saturated 1 M NaOH solution. As shown in Figure 3, Au catalysts generate approximately one-half of the limiting current density compared with that on Pt surface at the given oxygen concentration. It means that oxygen reduction partially occurs on bare Au surface with one-half number of electrons involved ($O_2 + H_2O + 2e^- \leftrightarrow HO_2^- + OH^-$). Typically, complete oxygen reduction ($O_2 + 2H_2O + 4e^- \rightarrow 4OH^-$) occurs on Pt catalysts.²⁸ However, oxygen reduction on the Au/AlPO₄ nanocomposites occurred with the steeper reduction slope as well as larger reduction current density in the potential region of approximately 0.8–1.0 V. The enhanced oxygen reduction including larger reduction current density was represented as newly appeared peak at ~0.85 V, and at the same time the oxidation peak at ~0.95 V disappeared on the reverse sweep. Typically, oxygen reduction in an alkaline solution undergoes the hydrogen peroxide intermediate state (step 1: $O_2 + H_2O + 2e^- \leftrightarrow HO_2^- + OH^-$; step 2: $HO_2^- + OH^- + H_2O + 2e^- \leftrightarrow 4OH^-$), according to Anastasijevic et al.'s model.²⁹ The hydrogen peroxides (HO_2^-) remain in the case of partial reduction of oxygen. To achieve the larger reduction current at the given oxygen concentration, the hydrogen peroxides should be reduced further to hydroxyl ions (OH^-). Therefore, the appeared peak at ~0.85 V with larger current density suggests that hydrogen peroxides (HO_2^-) were consumed and more feasible oxygen reduction occurred.³⁰ As seen on the reverse sweep, the oxidation peak at ~0.95 V is indicative of oxidation of the residual HO_2^- .³¹ The increased reduction of HO_2^- to OH^- on the Au/AlPO₄ nanocomposites leads to the decreased amount of HO_2^- oxidation in the cyclic voltammetry.

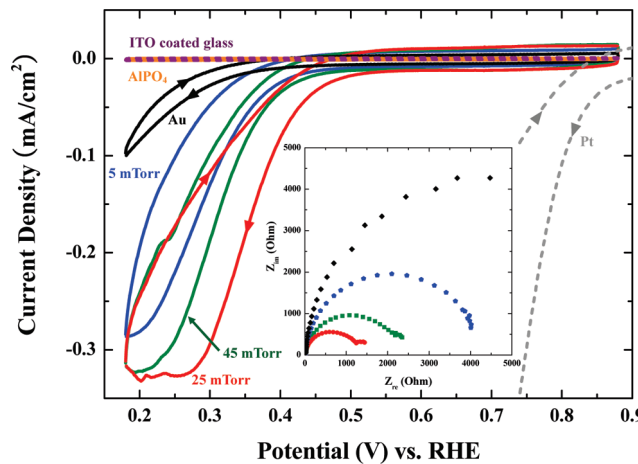


Figure 4. Oxygen-reduction activities of the Au/AlPO₄ nanocomposite, Au, and AlPO₄ electrodes in the oxygen-saturated 0.5 M H₂SO₄ solution at a scan rate of 50 mV/s. The inset is a Nyquist plot for the corresponding samples at 0.38 V.

$4e^- \leftrightarrow 4OH^-$) occurs on Pt catalysts.²⁸ However, oxygen reduction on the Au/AlPO₄ nanocomposites occurred with the steeper reduction slope as well as larger reduction current density in the potential region of approximately 0.8–1.0 V. The enhanced oxygen reduction including larger reduction current density was represented as newly appeared peak at ~0.85 V, and at the same time the oxidation peak at ~0.95 V disappeared on the reverse sweep. Typically, oxygen reduction in an alkaline solution undergoes the hydrogen peroxide intermediate state (step 1: $O_2 + H_2O + 2e^- \leftrightarrow HO_2^- + OH^-$; step 2: $HO_2^- + OH^- + H_2O + 2e^- \leftrightarrow 4OH^-$), according to Anastasijevic et al.'s model.²⁹ The hydrogen peroxides (HO_2^-) remain in the case of partial reduction of oxygen. To achieve the larger reduction current at the given oxygen concentration, the hydrogen peroxides should be reduced further to hydroxyl ions (OH^-). Therefore, the appeared peak at ~0.85 V with larger current density suggests that hydrogen peroxides (HO_2^-) were consumed and more feasible oxygen reduction occurred.³⁰ As seen on the reverse sweep, the oxidation peak at ~0.95 V is indicative of oxidation of the residual HO_2^- .³¹ The increased reduction of HO_2^- to OH^- on the Au/AlPO₄ nanocomposites leads to the decreased amount of HO_2^- oxidation in the cyclic voltammetry.

The oxygen reduction activities were also measured in an oxygen-saturated 0.5 M H₂SO₄ solution, as shown in Figure 4. The Au/AlPO₄ nanocomposites exhibit higher onset potential and steeper reduction slope than that of the Au catalyst. The Au/AlPO₄ nanocomposite deposited at 25 mTorr presents higher activity than other nanocomposites. Enhanced oxygen-reduction activities were also identified with the electrochemical impedance spectroscopy at 0.38 V. The overall activities of Au-based catalysts were low in an acidic environment. Typically, only partial oxygen reduction ($O_2 + 2H^+ + 2e^- \leftrightarrow H_2O_2$) occurs on the Au catalysts in an acidic solution.³² Abundant proton environment enables the protonation of HO_2^- to H_2O_2 , and the ORR does not proceed further. In addition, the activities of Au-free AlPO₄ were investigated as shown in Figure S3. In the alkaline environment, AlPO₄ itself was slightly active on the oxygen-reduction reaction. However, AlPO₄ had little oxygen-reduction activities in the acidic environment. The activities of AlPO₄ deposited at 25 mTorr in each environment were presented in Figures 3 and 4.

The XPS spectra for core levels of Au and the Au/AlPO₄ nanocomposite are shown in Figures 5a and S4. In the Au/AlPO₄

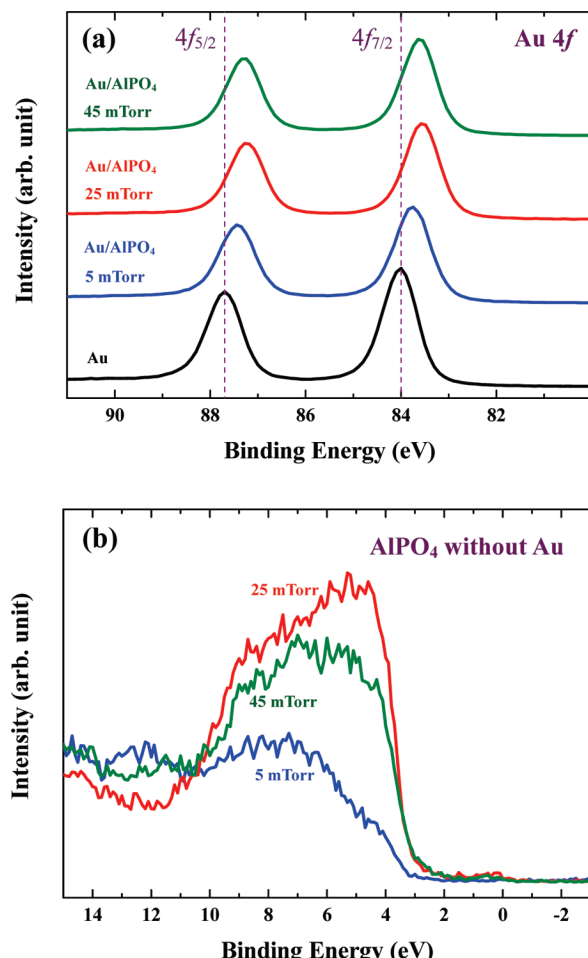


Figure 5. XPS of (a) the Au 4f region for the Au and Au/AlPO₄ nanocomposite electrodes and (b) the valence band region of AlPO₄ thin film with the Fermi energy at a 0 eV binding energy. The dashed lines indicate the peak positions of the 4f_{7/2} and 4f_{5/2} levels at 84.0 and 87.7 eV, respectively.^{35,36} Valence band spectra of AlPO₄ were comparable with the calculated density of state.³⁷

nanocomposite, the shift of the Au 4f peaks occurs toward lower binding energies, indicating the presence of a negative charge on the gold nanocrystallites due to the electron transfer from the AlPO₄ matrix material. Figure 5b shows that the valence band structure of AlPO₄ thin films without Au depends on the varied deposition condition. These changes are also related to the difference in the pseudolattice aluminum vibrational bands³³ in FT-IR of Figure S5. This is mainly from the nanostructural changes in the vicinity of the aluminum sites, and the electronic structure of aluminum phosphate is affected as well. It is estimated that various states of sputtered species at different operating pressures influence the chemical configuration and valence band structure of the deposited AlPO₄ compound. The equilibrium of electrons is attained by charge transfer from the varied valence band of AlPO₄ to the adjacent gold nanocrystallites, which is determined by the Fermi level.³⁴ The electron transfer between Au and AlPO₄ can modify the electronic structure of Au, and thereby affecting the catalytic activities of the oxygen reduction on the Au surface. It has been reported that the O–O bond of oxygen on the negatively charged gold nanoparticles is weakened and dissociated.^{14,15} As seen in Figures 3 and 4, the electron transfer to the gold nanocrystallites enhances the ORR catalytic activity.

Conclusions

Various Au/AlPO₄ nanocomposites were synthesized, in which ~10 nm gold crystallites were aggregated with AlPO₄. Catalytic activities of the prepared Au/AlPO₄ nanocomposites were examined for the ORR in an alkaline or acidic media. In the alkaline media, more feasible reaction existed within the region of approximately 0.8–1.0 V. In the acidic media, the onset potential of Au/AlPO₄ nanocomposite deposited at 25 mTorr was higher than the Au catalysts by ~0.2 V. Despite negligible activities of Au-free AlPO₄ on oxygen, the combination of Au and AlPO₄ remarkably enhanced the oxygen reduction. It is believed that the electron transfer from AlPO₄ to Au plays an important role in controlling the Au catalytic activities with the modification of electronic structure. The oxygen-reduction catalytic activities can be increased further by optimizing the nanostructures and interfaces of the Au/AlPO₄ nanocomposite.

Acknowledgment. This research was supported by the National Research Foundation of Korea, through the Research Center for Energy Conversion and Storage (RCECS, R11-2002-102-00000-0) and the World Class University (WCU, R31-2008-000-10075-0). We thank the National Center for Inter-University Research Facilities for XPS measurements, Center for Organic Light Emitting Diode for permitting UV absorption measurements, Center for Materials of Advanced Batteries for permitting FT-IR measurements, and UK Sim for AFM measurements.

Supporting Information Available: Additional characterizations (AFM, FT-IR, cyclic voltammograms, and XPS of Al 2s, P 2p, and O 1s). This material is available free of charge via the Internet at <http://pubs.acs.org>.

References and Notes

- (1) Steele, B. C. H.; Heinzel, A. *Nature* **2001**, *414*, 345–352.
- (2) Roychowdhury, C.; Matsumoto, F.; Zeldovich, V. B.; Warren, S. C.; Mutolo, P. F.; Ballesteros, M.; Wiesner, U.; Abruna, H. D.; DiSalvo, F. J. *Chem. Mater.* **2006**, *18*, 3365–3372.
- (3) Carrette, L.; Friedrich, K. A.; Stimming, U. *Fuel Cells* **2001**, *1*, 5–39.
- (4) Cheng, H.; Scott, K.; Lovell, K. *Fuel Cells* **2006**, *5*, 367–375.
- (5) Bunazawa, H.; Yamazaki, Y. *J. Power Sources* **2008**, *182*, 48–51.
- (6) Gonzalez, M. J.; Hable, C. T.; Wrighton, M. S. *J. Phys. Chem. B* **1998**, *102*, 9881–9890.
- (7) Luo, J.; Njoki, P. N.; Lin, Y.; Wang, L.; Zhong, C. *J. Electrochem. Commun.* **2006**, *8*, 581–587.
- (8) Xia, D.; Chen, G.; Wang, Z.; Zhang, J.; Hui, S.; Ghosh, D.; Wang, H. *Chem. Mater.* **2006**, *18*, 5746–5749.
- (9) Maruyama, J.; Abe, I. *Chem. Mater.* **2005**, *17*, 4660–4667.
- (10) Kim, C.; Park, Y.; Nahm, C.; Park, B. *Electron. Mater. Lett.* **2008**, *4*, 75–77.
- (11) Haruta, M. *Catal. Today* **1997**, *36*, 153–166.
- (12) Baker, W. S.; Pietron, J. J.; Teliska, M. E.; Bouwman, P. J.; Ramaker, D. E.; Swider-Lyons, K. E. *J. Electrochem. Soc.* **2006**, *153*, A1702–A1707.
- (13) Venezia, A. M.; Pantaleo, J.; Longo, A.; Carlo, G. D.; Casaletto, M. P.; Liotta, F. L.; Deganello, G. *J. Phys. Chem. B* **2005**, *109*, 2821–2827.
- (14) Yoon, B.; Häkkinen, H.; Landman, U.; Wörz, A. S.; Antonietti, J.-M.; Abbet, S.; Judai, K.; Heiz, U. *Science* **2005**, *307*, 403–407.
- (15) Sanchez, A.; Abbet, S.; Heiz, U.; Schneider, W.-D.; Häkkinen, H.; Barnett, R. N.; Landman, U. *J. Phys. Chem. A* **1999**, *103*, 9573–9578.
- (16) Cheetham, A. K.; Férey, G.; Loiseau, T. *Angew. Chem., Int. Ed.* **1999**, *38*, 3268–3292.
- (17) Lee, B.; Kim, C.; Park, Y.; Kim, T.-G.; Park, B. *Electrochim. Solid-State Lett.* **2006**, *9*, E27–E30.
- (18) Kim, C.; Lee, B.; Park, Y.; Park, B.; Lee, J.; Kim, H. *Appl. Phys. Lett.* **2007**, *91*, 113101.
- (19) Park, Y.; Lee, B.; Kim, C.; Kim, J.; Park, B. *J. Mater. Res.* **2009**, *24*, 140–144.
- (20) Yamamura, Y.; Ishida, M. *J. Vac. Sci. Technol. A* **1995**, *13*, 101–112.

- (21) Juodkazis, K.; Juodkazyte, J.; Šebeka, B.; Lukinskas, A. *Electrochim. Commun.* **1999**, *1*, 315–318.
- (22) Patterson, A. L. *Phys. Rev.* **1939**, *56*, 978–982.
- (23) Zorn, G.; Gotman, I.; Gutmanas, E. Y.; Adadi, R.; Salitra, G.; Sukenik, C. N. *Chem. Mater.* **2005**, *17*, 4218–4226.
- (24) Prikulis, J.; Hanarp, P.; Olofsson, L.; Sutherland, D.; Käll, M. *Nano Lett.* **2004**, *4*, 1003–1007.
- (25) Liz-Marzán, L. M. *Langmuir* **2006**, *22*, 32–41.
- (26) Myroshnychenko, V.; Carbó-Argibay, E.; Pastoriza-Santos, I.; Pérez-Juste, J.; Liz-Marzán, L. M.; Javier García de Abajo, F. *Adv. Mater.* **2008**, *20*, 4288–4293.
- (27) Prez, M. D.; Otal, E.; Bilmes, S. A.; Soler-Illia, G. J. A. A.; Crepaldi, E. L.; Grosso, D.; Sanchez, C. *Langmuir* **2004**, *20*, 6879–6886.
- (28) Markovic, N. M.; Gasteiger, H. A.; Ross, P. N., Jr. *J. Phys. Chem.* **1996**, *100*, 6715–6721.
- (29) Anastasijevic, N. A.; Vesovic, V.; Adzic, R. R. *J. Electroanal. Chem.* **1987**, *229*, 305–316.
- (30) Hernandez, J.; Solla-Gullon, J.; Herrero, E.; Aldaz, A.; Feliu, J. M. *J. Phys. Chem. C* **2007**, *111*, 14078–14083.
- (31) Strbac, S.; Adzic, R. R. *J. Electroanal. Chem.* **1996**, *403*, 169–181.
- (32) Shao, M. H.; Adzic, R. R. *J. Phys. Chem. B* **2005**, *109*, 16563–16566.
- (33) Rokita, M.; Handke, M.; Mozgawa, W. *J. Mol. Struct.* **2000**, *555*, 351–356.
- (34) Bube, R. H. *Electrons in Solids*; Academic Press, Inc.: San Diego, CA, 1992.
- (35) Takahiro, K.; Oizumi, S.; Terai, A.; Kawatsura, K.; Tsuchiya, B.; Nagata, S.; Yamamoto, S.; Naramoto, H.; Narumi, K.; Sasase, M. *J. Appl. Phys.* **2006**, *100*, 084325.
- (36) Moulder, J. F.; Stickle, W. F.; Sobol, P. E.; Bomben, K. D. *Handbook of X-Ray Photoelectron Spectroscopy*; Perkin-Elmer Corporation: Eden Prairie, MN, 1992.
- (37) Ching, W. Y.; Rulis, P. *Phys. Rev. B* **2008**, *77*, 125116.
- (38) Rotole, J. A.; Sherwood, P. M. A. *Surf. Sci. Spectra* **1998**, *5*, 60–66.
- (39) Murakami, Y.; Ijima, A.; Ward, J. W. *New Developments in Zeolite Science and Technology*; Elsevier: Amsterdam, 1986; Vol. 28.
- (40) Yu, J.; Xu, R. *Acc. Chem. Res.* **2003**, *36*, 481–490.
- (41) Mekky, W.; Nicholson, P. S. *J. Mater. Process. Technol.* **2007**, *190*, 393–396.

JP9103323

Modification of Gold Catalysis with Aluminum Phosphate for Oxygen-Reduction Reaction

Abstract | Supporting Info

Yejun Park, Byungjoo Lee, Chunjoong Kim, Jongmin Kim, Seunghoon Nam, Yuhong Oh and Byungwoo Park

pp 3688-3692

Publication Date (Web): February 10, 2010 (Article)

DOI: 10.1021/jp9103323

Full Text HTML

Hi-Res PDF [2971K]

PDF w/ Links [255K]

Subscriber Access

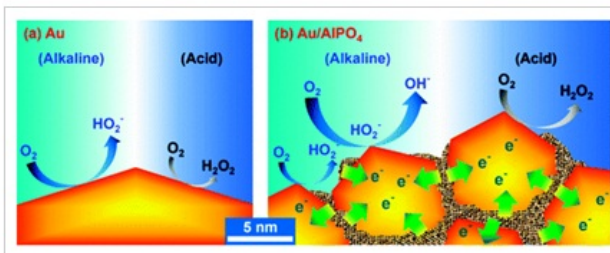


Figure 1 of 6

» Next

Structural, Electronic, and Electrochemical Properties of Cathode Materials Li₂MSiO₄ (M = Mn, Fe, and Co): Density Functional Calculations

Abstract | Supporting Info

Guohua Zhong, Yanling Li, Peng Yan, Zhuang Liu, Maohai Xie and Haiqing Lin

pp 3693-3700

Publication Date (Web): February 5, 2010 (Article)

DOI: 10.1021/jp910746k

Full Text HTML

Hi-Res PDF [3215K]

PDF w/ Links [496K]

Subscriber Access

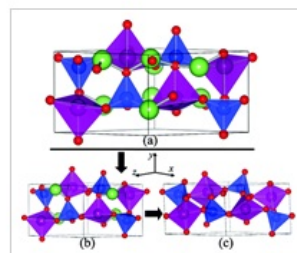


Figure 1 of 8

» Next

Solution-Processable Organic Molecule with Triphenylamine Core and Two Benzothiadiazole-Thiophene Arms for Photovoltaic Application

Abstract

Yi Yang, Jing Zhang, Yi Zhou, Guangjin Zhao, Chang He, Yongfang Li, Mattias Andersson, Olle Inganäs and Fengling Zhang

pp 3701-3706

Publication Date (Web): February 10, 2010 (Article)

DOI: 10.1021/jp910836t

Full Text HTML

Hi-Res PDF [2461K]

PDF w/ Links [237K]

Subscriber Access

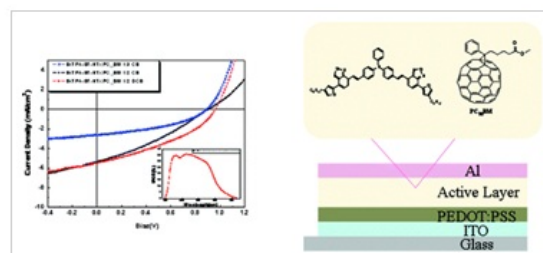


Figure 1 of 7

» Next